Morphology-dependent optical and wetting behavior of GLAD PTFE thin films

Rajnarayan De , **S. Maidul Haque, Ranveer Singh, C. B. Basak, S. Jena, J. S. Misal, D. D. Shinde, Tapobrata Som, K. Divakar Rao**

Abstract E-beam evaporation equipped with glancing angle deposition arrangement (GLAD) was used to fabricate nanostructured polytetrafluoroethylene (PTFE) films in a single-step coating process. Three sets of PTFE coatings were prepared using various oblique angles, e-beam currents, and deposition times to explore the effects of deposition parameters on the properties of PTFE nanostructured coatings. Water contact angle (WCA) of the coatings was found to be enhanced with the increase in all the above process parameters. Optical transmittance of the coatings was also found to be improved with the above parameters except for in the case of an increase in thickness of the films (in very high thickness region), where the transmittance was degraded due to light scattering from the sample surface. After all the optimizations, the $\sim$ 130-nm-thick GLAD PTFE sample prepared with highest e-beam current was found to be more suitable for antireflection and self-cleaning applications. The single-sided coating demonstrates a very high average transmittance of $\sim$ 95.6% (with a wideband transmittance spectrum among the others) in the visible and NIR wavelength range with excellent self-cleaning nature (WCA $\sim$ 156°, sliding angle $\sim$ 10°). The trend of measured WCA with respect to surface roughness follows the Cassie–Baxter model. Overall, the study demonstrates the possibility of fabricating highly transparent self-cleaning coatings using the GLAD technique, which is potentially useful for fabricating protecting cover glasses in solar panels.

Keywords PTFE, GLAD, Antireflection, Superhydrophobicity

R. De (✉), S. M. Haque, J. S. Misal,
D. D. Shinde, K. D. Rao
Photonics and Nanotechnology Section, Atomic and
Molecular Physics Division, Bhabha Atomic Research
Centre Facility, Visakhapatnam 531011, India
e-mail: rajde@barc.gov.in

R. De, C. B. Basak, T. Som, K. D. Rao
Homi Bhabha National Institute, Mumbai 400094, India

R. Singh, T. Som
Institute of Physics, Sachivalaya Marg, Bhubaneswar,
Odisha 751005, India

Present Address:
R. Singh
Department of Energy Systems Research, Ajou University,
Suwon 443-739, Republic of Korea

C. B. Basak
Mechanical Metallurgy Division, Bhabha Atomic Research
Centre, Mumbai 400085, India

S. Jena
Atomic and Molecular Physics Division, Bhabha Atomic
Research Centre, Mumbai 400085, India

Introduction

During the past few years, replicating naturally existing water-repellent surfaces (lotus leaf, butterfly wings, etc.) has drawn the attention of researchers.[1–5] These bio-inspired surfaces are extremely useful in many real-life applications like self-cleaning, antifogging, and antiicing.[6–9] On the other hand, coatings with bare minimum reflection losses are very important for applications where maximum light transmission is desired (e.g., solar cells, flat panel displays, etc.).[10–12] Surfaces placed in open air environment and coated with antireflective layers have a tendency to deteriorate their performance due to the accumulation of dust on the surfaces leading to reflection losses. This is a serious problem for solar cells, where after some time, the efficiency of the cell is degraded due to the dust particles settling on the top surface.[13–16] These prob-

lems provide an inspiration to the scientists to play with surface engineering of man-made coatings and produce surfaces that are simultaneously water-repellent and antireflecting.[17–20]

Antireflection coatings (ARCs) work with a very basic theory of achieving minimum light reflection from any material by reducing the refractive index contrast between the ambient and the material medium. Glass is a very popularly known material for optical applications due to its high transparency for wavelengths above 400 nm. However, a total of 8% reflection loss is inherently present due to the Fresnel's reflection from its surfaces. So, it is very important to recover this 8% loss in transparency of the glass in order to improve the efficiency of the underlying devices. Generally, ARCs are fabricated by depositing a multilayered stack of low and high index materials on the substrate surface,[10] but fabrication of such coatings often involves complex preparation processes. Hydrophobicity of solid surfaces is dependent on surface free energy and surface roughness. Usually, choosing materials having low surface free energy and creating controlled top surface roughness serve the purpose easily.

Generally, simultaneous production of superhydrophobic and antireflective surfaces is difficult due to the competitive nature of surface roughness and transmittance.[21] Creating surface roughness may be beneficial for superhydrophobicity, but it has a negative effect on transparency due to the enhancement of light scattering from the surface.[22] So, a balanced deposition condition is necessary.

Glancing angle deposition (GLAD) [an extreme case of oblique angle deposition (OAD)] is an efficient technique for fabricating antireflecting and water-repellent coatings due to its unique capability of producing tailored optical properties (i.e., refractive index) and surface morphology of thin films.[23] It uses the well-known self-shadowing effect to control the surface structure of the coatings. Although several other techniques are available which can generate antireflecting surfaces with hydrophobic characteristics, all techniques have their own limitations, such as complexity in the fabrication process, time-consuming deposition methods, and less control on process parameters involved.[24,25] Several reports are available on creating superhydrophobic and antireflecting surfaces using GLAD technique, but they failed to demonstrate both the antireflection and superhydrophobic characteristics at the same time.[26,27] Recently, in the work reported by Lu et al.,[28] GLAD technique has been used to prepare transparent superhydrophobic SiO$_2$ coatings (WCA $\sim$ 156°), but the transparency in their films was limited to only ($\sim$ 92%). The results show the potentiality of the GLAD technique in fabricating such multifunctional surfaces.

In our previous communication,[29] we fabricated highly transparent superhydrophobic coating of PTFE material. The films were prepared in normal deposition geometry, i.e., substrates were placed at 0° angle of incidence and depositions were taken at a very high deposition rate ($\sim$ 450 Å/s) that drastically reduced the control over process parameters in the fabrication process. To get rid of this problem, in our present study we tried to create similar surfaces but with optimized lower deposition rate (maximum 125 Å/s @ 20 mA e-beam current) to have better control. Here, we have introduced the GLAD technique, which can inherently enhance the surface roughness and serve the purpose of using very high deposition rate in the previous study partially. As fabrication of such multifunctional coatings often require a genuine selection of coating material, in both the studies we have used polytetrafluoroethylene as the coating material due to the low surface energy ($\sim$ 18.6 mN m^{-2}) and low refractive index ($\sim$ 1.38 @ 550 nm) inherently present in the material itself.

In the present study, we have explored the GLAD technique along with other important deposition parameters to demonstrate thin film coatings with high transparency and superhydrophobicity. We have attempted to improve the properties further by tailoring several deposition parameters including deposition angle, rate of deposition, and time of deposition. At the end, an optimized deposition condition has been selected that demonstrates both antireflecting and superhydrophobic properties simultaneously with a better control on the process parameters involved.

Experimental details

Fabrication of the nanostructured PTFE films

PTFE nanostructured coatings were fabricated on BK7 and Si (111) substrates (of area $\sim$ 5 cm^2) using electron beam evaporation technique (HHV make EB03) equipped with glancing angle deposition arrangement. During the deposition process, the substrates were mounted on a sample holder capable of tilting at any angle between 0 and 90° with respect to the incoming vapor flux. No azimuthal rotation was applied to the substrates during the coating process. Prior to deposition, the vacuum chamber was evacuated to a base vacuum level of $\sim$ 3 × 10^{-6} mbar using turbomolecular pump backed by a rotary pump and the depositions were carried out in the 10^{-4} mbar vacuum range. The distance between the evaporation source (Himedia make PTFE granules) and center of the substrate was fixed at 220 mm for all the depositions. Three sets of samples were prepared with varying (1) angle of deposition, (2) e-beam current, i.e., rate of deposition, and (3) film thickness. For set (1), thickness of the films was restricted to $\sim$ 100 ± 5 nm and depositions were carried out at 5 mA e-gun current with angle of deposition varied to 0°, 50°, 75°, and 86°. For preparing set (2), film thickness was restricted to 100 ± 5 nm and deposition angle was fixed at 86°, but the e-gun current

was varied to 10 and 20 mA to get enhanced deposition rates. For set (3), the e-gun current and deposition angle were fixed at 20 mA and 86°, respectively, but deposition time was varied to get varying thicknesses of the films.

Characterization of the films

The films prepared on BK7 substrate were used to measure the optical properties using spectroscopic ellipsometry, spectrophotometry, and water contact angle (WCA) using an indigenously developed WCA measurement setup. Thin films fabricated on Si (111) were utilized for surface morphology measurements using scanning electron microscopy (FE-SEM) and atomic force microscopy (AFM). As the coatings were prepared without any azimuthal rotation, all the characterizations (except WCA measurements) were carried out in the central region (few mm^2) of the substrates. However, WCA values were evaluated by taking measurements at different locations covering maximum area of the coated surface ($\sim$ 5 cm^2).

Spectroscopic ellipsometry measurements of the coatings were done using Semilab GES5-E rotating polarizer spectroscopic ellipsometer in the 200–900 nm wavelength range and at 70° angle of incidence. A detailed description of spectroscopic ellipsometry (SE) data analysis is already reported elsewhere.[30] The optical parameters of all the GLAD PTFE samples were evaluated from the SE data by assuming a bilayer film structure that consists of a bottom bulk-like layer and a top porous layer of PTFE.[30] The bottom layer was assumed to follow Cauchy's dispersion model,[31] and the top porous layer was analyzed by using Bruggeman effective medium approximation (EMA) model.[31] Since a bilayer film structure was assumed, a thickness weighted refractive index (n_{eff}) value of the two layers (i.e., bulk-like layer and top porous layer) was evaluated to demonstrate variation in optical properties of the specimens with varying deposition conditions.

Jasco V-630 spectrophotometer was utilized for optical transmittance measurement of the films in 200–1100 nm wavelength range.

Morphological characterization (both top and cross-sectional view mode) was done using field emission-based scanning electron microscope (FE-SEM) operated at 1 keV energy of electrons (without any conductive coating) and 20 KX magnification. Few samples were measured at 50 KX magnification scale to view the fine surface features present. MFP3D, Asylum Research (USA) atomic force microscope (AFM) was used to measure surface parameters of the samples.

The details of our indigenously developed WCA measurement setup have been reported elsewhere.[29] All the WCA measurements were taken with 4-μL water droplets of de-ionized water. For each WCA data point, five measurements were taken and the mean WCA values were plotted.

Results and discussion

Effect of deposition angle on the film properties

To explore the effect of deposition angle on the optical and wetting properties of the coatings, films were prepared at different oblique angles. Spectroscopic ellipsometry data analysis confirmed the thickness of the films to be 100 ± 5 nm.

From the optical transmittance measurements, it can be seen that all the films show an average transmittance of 94.5–95.0% in the visible wavelength range (as shown in Fig. 1a) with no significant improvement in transmittance with oblique angle. This can be explained by the effective refractive index (n_{eff}) values (shown in Fig. 1b) of the films evaluated from spectroscopic ellipsometry (SE) measurements. Although the film prepared at 0° oblique angle possesses the highest n_{eff} value, variation w.r.t. the other oblique angle deposited samples is not very significant. Less
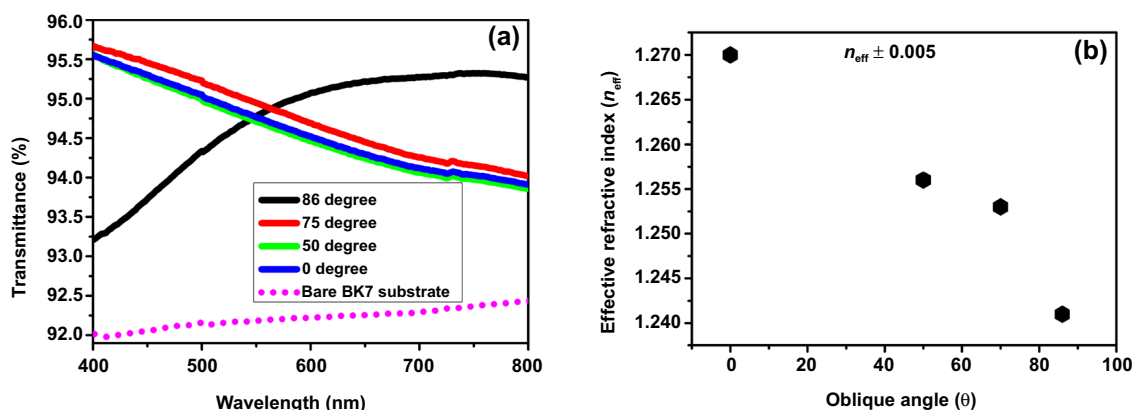

Fig. 1: (a) Optical transmittance data and (b) effective refractive index (@ 550 nm) of the PTFE thin films prepared with varying angle of deposition
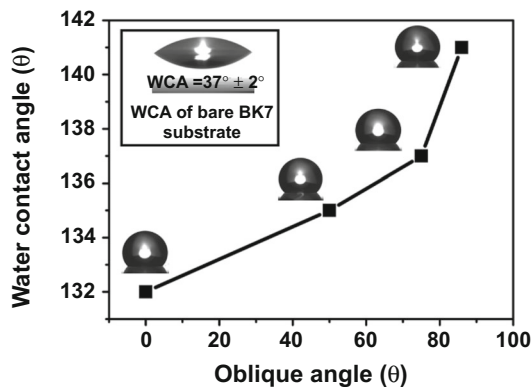
Fig. 2: **Variation of water contact angle with oblique angle of deposition. Inset shows WCA data of bare BK7 substrate for reference**
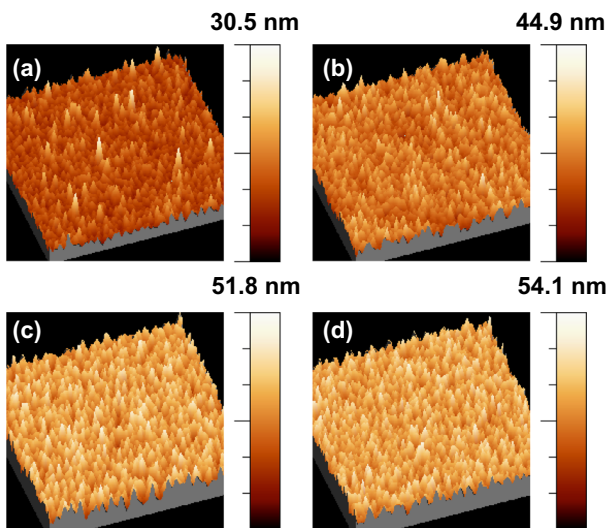

Fig. 3: **AFM topograph (2 μm × 2 μm) of PTFE samples deposited at varying oblique angles (a) 0°, (b) 50°, (c) 75°, and (d) 86°**

Table 1: RMS roughness data of the films prepared at different oblique angles

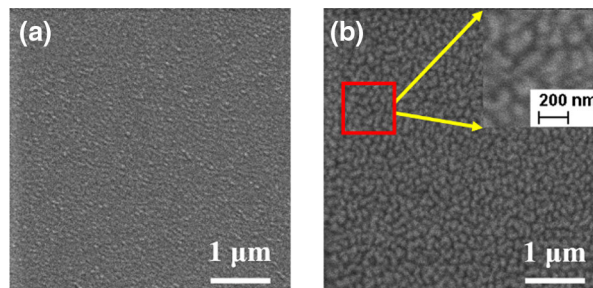| Deposition condition (oblique angle in degree)	RMS roughness (nm)
0	2.9
50	5.0
75	7.1
86	7.3

Fig. 4: **FE-SEM images (top view) of the PTFE samples prepared at (a) 0° and (b) 86° oblique angles**

(2 μm × 2 μm) of the films prepared at varying angles of deposition. It can be seen from the roughness data (extracted from AFM data shown in Fig. 3) presented in Table 1 that the relative increase in RMS roughness value is more for higher oblique angle values leading to higher WCA values in the films. It is well known that films prepared at 0° angle of deposition form a compact film structure due to mobility induced diffusion of incident adatoms on the substrate surface. Hence, the film tends to show small RMS roughness values. However, the situation alters with the increase in angle of deposition. For higher deposition angles, not all the sites on the substrate surface are accessible to the arrived adatoms due to the self-shadowing effect. During the initial stages of film growth, the vapor species nucleate at random locations on the substrate. As growth continues, more flux gets accumulated in these locations and shadowed regions are formed behind them. This restricts film growth in the shadowed locations. Hence, a porous and rough film structure is formed. This leads to an increase in RMS roughness in film morphology.

Two representative top view FE-SEM images of the samples are shown in Fig. 4. It can be seen from Fig. 4a that the film prepared at 0° oblique angle has a fine compact grain structure. With the increase in oblique angle to 86° (Fig. 4b), surface features become visible.

The occurrence of these nanofeatures is solely due to the shadowing effect caused by the glancing angle deposition arrangement. Usually, films prepared at higher oblique angle values show better surface features compared to continuous bulk-like coatings prepared at normal geometry due to the limited

variation in the n_{eff} value among the samples results in less variation in the average optical transmittance of the specimens. A shift in maximum transmittance wavelength region for the 86° deposited sample was observed that may be due to the highest thickness of the specimen among the others.

The water contact angle data presented in Fig. 2 shows improvement in hydrophobic quality of the coatings with oblique angle. This increase is caused by the morphological alterations that occurred (i.e., increase in rms surface roughness) in the films with angle of deposition. The same is reflected in the WCA data also.

It is well known that the water repellency of a hydrophobic coating can be enhanced by increasing its surface roughness. Figure 3 shows AFM images

surface diffusion of the adatoms on the substrate surface. So, finally the oblique angle of 86° was selected to be the optimum deposition condition as the coating shows highest WCA of $\sim 141° \pm 2°$ among the others with equivalent optical transmittance. A study by Lu et al.[28] for GLAD SiO_2 films has also reported a similar trend in WCA with oblique angle of deposition.

Effect of e-beam current on the films

Rate of deposition can play a crucial role in deciding the film RMS roughness and thereby the hydrophobic nature of the films. In e-beam evaporation technique, the deposition rate can be controlled by e-beam current which manipulates the rate of evaporation in the deposition process. In the present work, the e-beam current was varied after fixing the oblique angle at 86° to achieve more deposition rate in the film growth process. Thickness of the films was restricted to 100 ± 5 nm for all depositions. It is confirmed from the results shown in previous section that though the film prepared at 86° oblique angle shows the highest WCA, it may not be possible to improve further by only depending on the oblique angle parameter.

The optical transmittance data presented in Fig. 5a clearly show the effect of varying e-beam current on film transmittance. It can be seen that the film deposited at 20 mA e-beam current shows highest transmittance with peak value $\sim 96.0\%$ and average value $\sim 95.6\%$, which is the best possible result achieved with a single-sided antireflection coating on glass. This can be explained by the enhanced porosity fraction introduced in the film structure due to increased deposition rate because of increasing e-beam current. The film porosity plays a key role in deciding the effective refractive index (n_{eff}) of the film.

It can be seen from Fig. 5b that with the increase in e-beam current from 5 to 20 mA, the effective refractive index of the coating decreases. An increase in e-beam current enhances the rate of deposition (men-tioned in Table 2). So, the arrived vapor species do not get sufficient time to settle in minimum surface energy positions. This introduces voids in film and thereby produces a porous film structure.[30] The enhanced porosity of the coatings can be clearly seen from the FE-SEM images presented in Fig. 6.

The film prepared at 20 mA e-beam current shows a more well-separated grain structure distribution compared to that deposited with 5 mA. An improvement in water repellency of the films is also visible in the WCA data shown in Fig. 7.

WCA of the coatings is increased from $141° \pm 2°$ to $155° \pm 2°$ by increasing the e-beam current. The trend can be corroborated with the AFM data shown in Fig. 8. RMS roughness values of the films are listed in Table 2. It is clear that the RMS roughness is substantially enhanced due to the increased deposition rate. The effect of this enhanced surface roughness is visible in the WCA data of the coatings.

So, it can be concluded from the analysis that the film fabricated with 20 mA e-beam current is more effective in repelling water on the coating surface and also shows antireflecting property. A similar trend was also found in the report by Lu et al.[28] for GLAD SiO_2 films where a higher deposition rate (~ 10 Å/s) was selected with better WCA value. Effect of e-beam currents beyond 20 mA was not explored due to the reduction in deposition time, i.e., loss of control on the process.

Table 2: RMS roughness data of the films prepared at different oblique angles

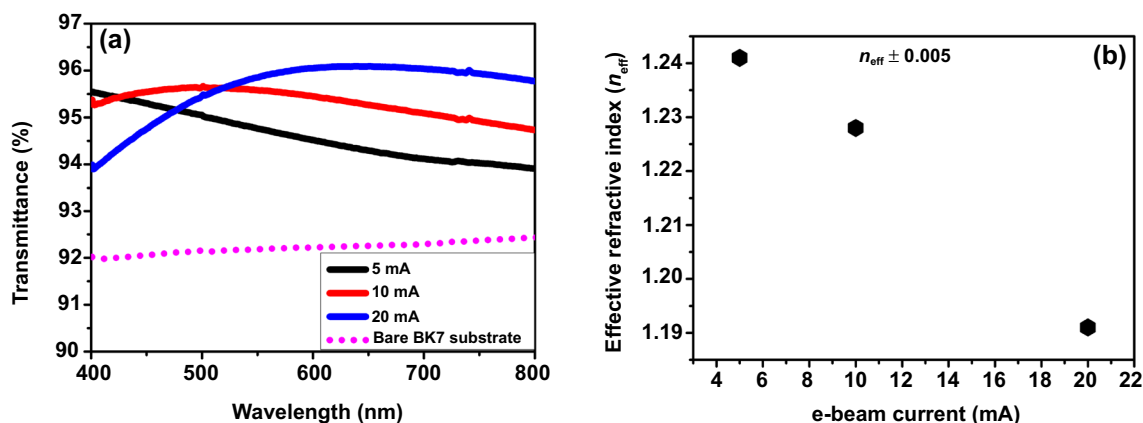| Deposition condition (e-beam current in mA/Deposition rate)	RMS roughness (nm)
5 (~ 71 Å/s)	7.3
10 (~ 84 Å/s)	8.7
20 (~ 125 Å/s)	16.0

Fig. 5: (a) Optical transmittance data and (b) effective refractive index (@ 550 nm) of the GLAD PTFE films prepared with varying e-beam current

Effect of film thickness on WCA and transmittance of the coatings

To investigate the effect of thickness on the optical and water wetting properties of the samples, GLAD PTFE films of different thicknesses (viz. 100, 130, 150, 180, and 300 nm) were fabricated. Depositions were taken at the optimum deposition conditions of deposition angle at 86° and e-beam current adjusted to 20 mA. Representative AFM images of the samples are presented in Fig. 9.

It can be seen from Fig. 9 that as the film thickness is increased from 100 to 300 nm, maximum height of the surface structures also increased from 123.3 to 180.3 nm. As a result, RMS roughness value reached a highest value of ~ 24 nm.[32] The effect of this increase is seen in the WCA data shown in Fig. 10, where the 300-nm-thick sample shows the highest WCA of $\sim 164° \pm 2°$ with no significant variation in WCA value observed for the samples with thicknesses of 100, 130, and 150 nm. This result is comparable with the WCA value reported in our previous communication where the films were deposited at zero oblique angle and extremely high deposition rate.[29]

Although the enhanced film thickness shows a positive effect in water repellency of the coatings, the scenario is opposite for the case of optical transmit-

tance of the coatings (as shown in Fig. 11a). Optical transmittance plot of the 130-nm-thick specimen is flatter (i.e., wideband) compared to the 100-nm-thick sample with negligible variation in average transmittance ($\sim 95.6\%$). This degradation in optical transmittance for films with higher thicknesses (150 nm and higher) is probably caused by the scattering of light incident on the sample surface together with the enhanced effective refractive index and thickness of the specimen.

A similar trend was also observed in effective refractive index of the coatings (shown in Fig. 11b) with the increase in film thickness. It can be seen that n_{eff} value of the coatings increases with the increase in film thickness and a maximum value observed for 300-nm-thick GLAD PTFE specimen. With the increase in film thickness, the nearby columns coalesce due to broadening of nanocolumns and produce a less porous film structure.[33] A clear difference in transparency as well as WCA of the best performing ~ 130-nm-thick GLAD PTFE sample from uncoated BK7 substrate is also visible in the photograph shown in Fig. 11c. The uncoated substrate shows a high reflection of the

Fig. 8: AFM morphographs (2 μm × 2 μm) of GLAD PTFE samples deposited at varying e-beam currents (a) 5 mA, (b) 10 mA, and (c) 20 mA
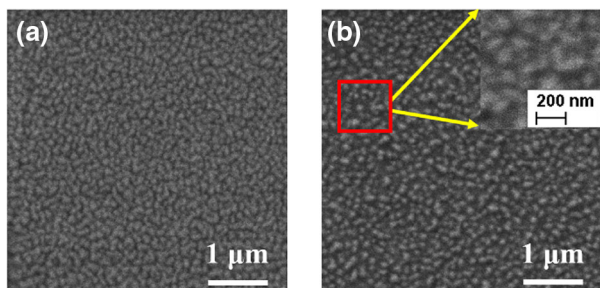
Fig. 6: FE-SEM images (top view) of the GLAD PTFE films prepared at (a) 5 mA and (b) 20 mA e-beam current
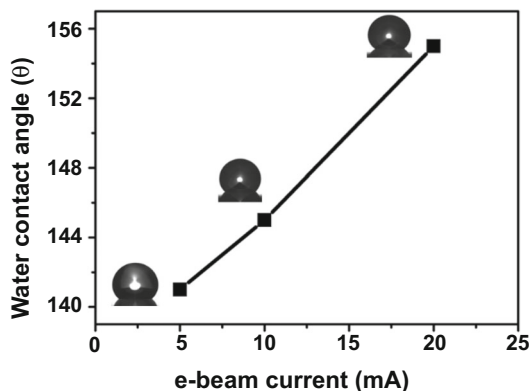
Fig. 7: Effect of varying e-beam current on WCA of the GLAD PTFE coatings
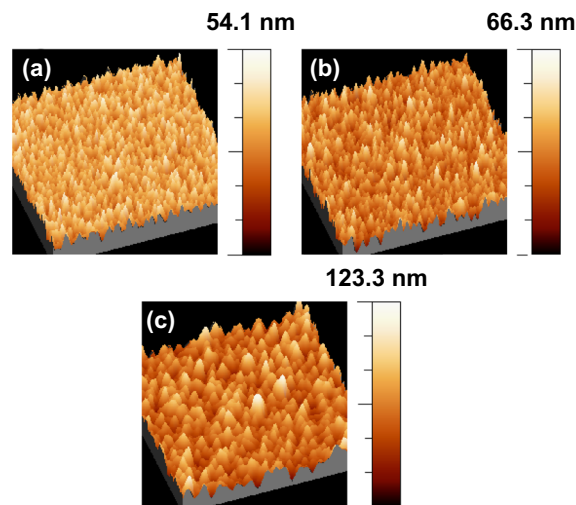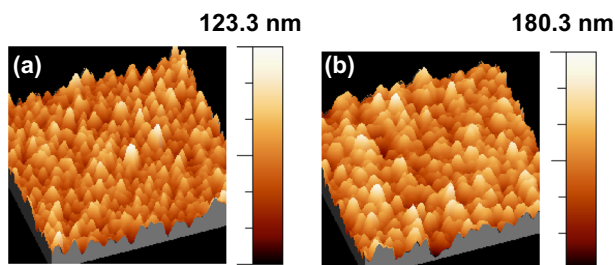
Fig. 9: Representative AFM images (2 μm × 2 μm) of the samples of different thicknesses (a) 100 nm and (b) 300 nm

incident white light together with water droplet spread over compared to the coated sample.

It can be seen from Fig. 12 that the 100-nm-thick sample shows well-separated grain structures, whereas the sample with 300 nm thickness (b and c) value has network-type surface texture with dimension nearly equal to the incident light wavelength.

Although the vertical features present in the film have dimension which do not match with light scatter-
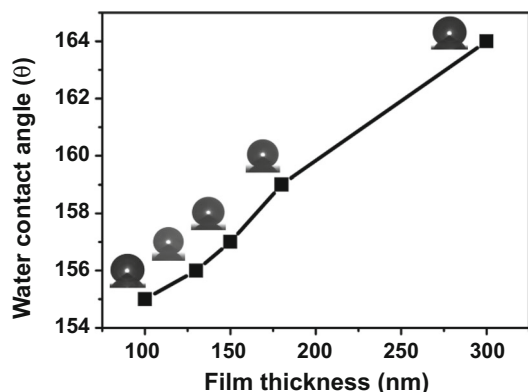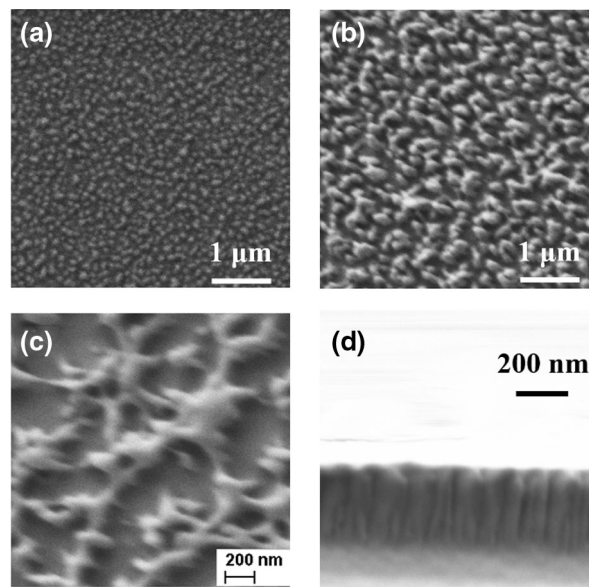

Fig. 12: Top view FE-SEM data of the GLAD PTFE coatings prepared with different thicknesses (a) 100 nm, (b) 300 nm @ 20KX magnification, (c) 300 nm @ 50KX magnification, and (d) cross-sectional FE-SEM data of 300-nm-thick sample

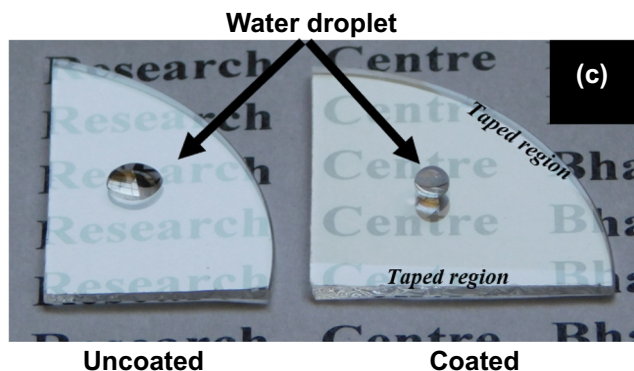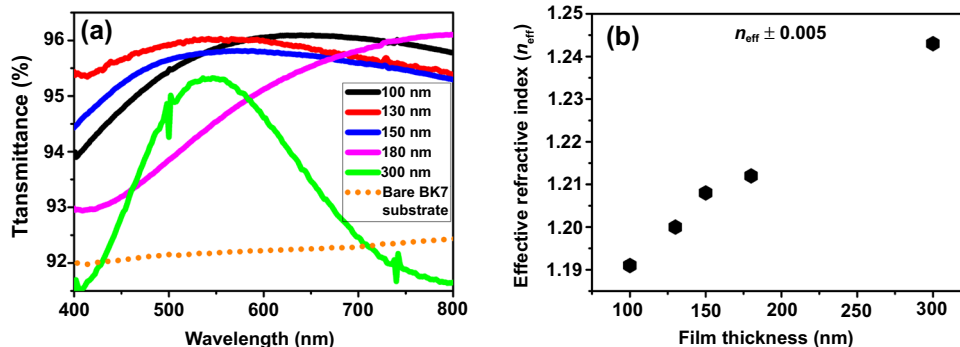Fig. 10: Effect of varying film thickness on WCA of the GLAD PTFE coatings

Fig. 11: (a) Optical transmittance data and (b) effective refractive index (@ 550 nm) of the GLAD PTFE coatings prepared with varying thicknesses; (c) photograph of uncoated substrate and the best performing GLAD PTFE ($\sim$ 130-nm-thick) coated sample
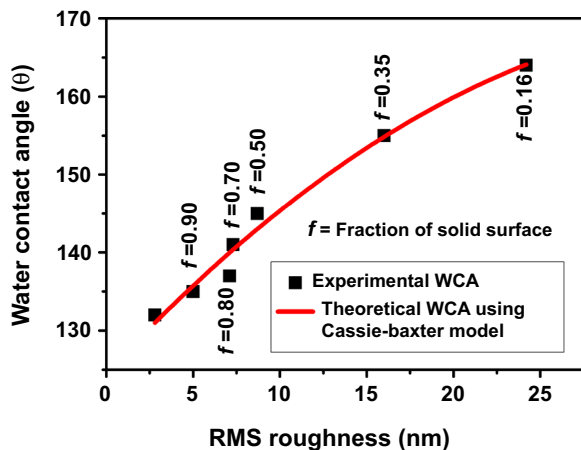
Fig. 13: The variation of WCA of the PTFE thin films with RMS surface roughness and theoretical WCA values predicted by Cassie–Baxter model

ing criteria (in the visible wavelength range), scattering can occur from the lateral features present on the film surface. The cross-sectional FE-SEM data for 300-nm-thick sample (shown in Fig. 12d) shows nanorod-like structures representing columnar growth of films in glancing angle deposition technique.

Based on these results, the samples prepared with very high thickness values are not suitable for practical applications as these coatings fail to show antireflecting and superhydrophobic nature simultaneously. The film prepared at 20 mA e-beam current and thickness having $\sim$ 130 nm is found to show best performance among the others. The same coating shows excellent water-repellent property with WCA $\sim$ 156° $\pm$ 2° and a wideband transmittance spectrum with $\sim$ 3.6% higher transmittance than the BK7 glass substrate (used in the study) in the entire visible wavelength spectrum. The uniformity of the final optimized GLAD PTFE sample (i.e., $\sim$ 130 nm thick) deposited on an area of $\sim$ 5 cm^2 was evaluated by measuring optical transmittance, thickness, and water contact angle (WCA) of the sample at various locations on the sample surface. Spectroscopic ellipsometry (SE) data analysis revealed a thickness variation of $\pm$ 2% with an average transmission variation of 0.3%, confirmed from the optical transmission measurements. WCA variation in the sample was $\pm$ 2°.

Mechanical durability of the $\sim$ 130-nm-thick GLAD PTFE specimen prepared at 20 mA e-beam current was tested using two conventional mechanical robustness tests, viz. underwater ultrasonication test and long-time water immersion test.[34,35] Both the tests resulted in negligible variation in average transmittance (i.e., 95.6%) of the coating. However, variation in WCA of the coating was noticed in both the tests. The long-time water immersion test (performed by dipping the specimen for 5 h in de-ionized water) resulted in a reduced WCA of the specimen to $\sim$ 145° $\pm$ 2°. WCA of the specimen was also found to decrease

to $\sim$ 131° $\pm$ 2° in the underwater ultrasonication test (performed by ultrasonicating the specimen in de-ionized water for 30 min in room temperature).

Sliding angle (SA) of the same GLAD PTFE coating ($\sim$ 130 nm thick) was also determined by fixing the sample on a tilt stage. SA of the specimen was measured to be the particular tilt angle of the stage where the static water droplet rolls off on the surface. The measured SA of the sample was found to be $\sim$ 10° $\pm$ 0.2°, which is comparable with the SA values reported in the literature.[36,37]

Theoretical calculation of WCA on the rough surfaces

There are two well-established theoretical models to explain water wettability of rough surfaces: Wenzel model[38] and Cassie–Baxter model.[39] In the present study, we have calculated the WCA for all the films using the Cassie–Baxter theoretical model (as also reported in other studies[28]). Figure 13 demonstrates the experimental and theoretically obtained WCA values of the films with their respective RMS roughness as well as fraction of solid surface.

The theoretical WCA (θ_c) for the Cassie–Baxter model is as follows:

$$\cos \theta_c = f(\cos \theta_0 + 1) - 1$$

where θ_0 is the measured WCA of the ideal flat surface and f is the fraction of solid surface, i.e., the top area of the nanostructured grains.

In the present study, the fraction of solid surface of each sample was calculated using AFM image analysis (as indicated in Fig. 13). The individual grains were marked using "threshold" and "watershed" algorithms of Gwyddion AFM analysis software.[40] Then, WCAs of the samples were evaluated using the equation mentioned above. The measured WCA of flat PTFE surface (θ_0) was taken to be 132°, i.e., the value measured for the sample prepared at 0° oblique angle. Finally, the theoretically obtained WCA values were fitted using a polynomial fitting algorithm. It can be seen from the figure that the measured WCAs of the films are in good agreement with the predicted theoretical values.

Conclusions

In the present communication, a systematic investigation has been carried out to find the optimum deposition parameters suitable for making antireflecting superhydrophobic PTFE coatings in a single step using oblique angle deposition technique. In the first set, the effect of oblique angle on the film properties was explored and an optimum angle of 86° (glancing angle)

was decided. Using this knowledge of optimum deposition angle, further experiments were conducted and a second set of samples were prepared with varying e-beam current (i.e., rate of deposition). Improvement in optical transparency and water repellency of the coatings was noted with the increase in e-beam current. To further improve the results, a third set was prepared with different film thickness values by controlling the time of deposition. Though the coatings with very high thicknesses ($\sim$ 300 nm) showed enhanced WCA values (i.e., improved hydrophobic quality), optical transparency was found to be decreased due to the enhanced light scattering from the coating surface together with an increased effective refractive index of the coatings. However, the 130-nm-thick specimen of the third set showed a flatter transmittance spectrum in the visible and NIR ranges (400–800 nm) with highest average transmittance ($\sim$ 95.6%) and WCA ($\sim$ 156°) among the others. So, the 130-nm-thick GLAD-PTFE sample deposited at 86° angle of incidence and 20 mA e-beam current was found to be the optimum coating among all three sets for simultaneous performance of high transparency and good water repellency. The same coating also showed a sliding angle (SA) value of $\sim$ 10°. A theoretical calculation of WCA of the samples was also done using Cassie–Baxter model. The measured WCAs of the films were found to be in agreement with the theoretical obtained values. As the coated device shows a wideband transmittance spectrum in the visible and NIR range with high transparency as well as good self-cleaning property, it may be of potential use in the production of cover glasses for solar panels, wind-shields in automobile industries, etc.

References

1. Barthlott, W, Neinhuis, C, "Purity of the Sacred Lotus, or Escape from Contamination in Biological Surfaces." *Planta*, **202** 1–8 (1997)

2. Fang, Y, Sun, G, Wang, TQ, Cong, Q, Ren, LQ, "Hydrophobicity Mechanism of Non-smooth Pattern on Surface of Butterfly Wing." *Chin. Sci. Bull.*, **52** 711–716 (2007)

3. Neto, AI, Meredith, HJ, Jenkins, CL, Wilker, JJ, Mano, JF, "Combining Biomimetic Principles from the Lotus Leaf and Mussel Adhesive: Polystyrene Films with Superhydrophobic and Adhesive Layers." *RSC Adv.*, **3** 9352 (2013)

4. McCarthy, M, Gerasopoulos, K, Enright, R, Culver, JN, Ghodssi, R, Wang, EN, "Biotemplated Hierarchical Surfaces and the Role of Dual Length Scales on the Repellency of Impacting Droplets." *Appl. Phys Lett.*, **100** 263701 (2012)

5. Bhushan, B, Jung, YC, "Natural and Biomimetic Artificial Surfaces for Superhydrophobicity, Self-cleaning, Low Adhesion, and Drag Reduction." *Prog. Mater. Sci.*, **56** 1–108 (2011)

6. Latthe, SS, Gurav, AB, Maruti, CS, Vhatkar, RS, "Recent Progress in Preparation of Superhydrophobic Surfaces: A Review." *J. Surf. Eng. Mater. Adv. Technol.*, **2** 76–94 (2012)

7. Gurav, AB, Latthe, SS, Vhatkar, RS, Lee, JG, Kim, DY, Park, JJ, Yoon, SS, "Superhydrophobic Surface Decorated with Vertical ZnO Nanorods Modified by Stearic Acid." *Ceram. Int.*, **40** 7151–7160 (2014)

8. Zhang, XY, Li, Z, Liu, KS, Jiang, L, "Bioinspired Multifunctional Foam with Self-cleaning and Oil/Water Separation." *Adv. Funct. Mater.*, **23** 2881–2886 (2013)

9. Wang, YY, Xue, J, Wang, QJ, Chen, QM, Ding, JF, "Verification of Icephobic/Anti-icing Properties of a Superhydrophobic Surface." *ACS Appl. Mater. Interfaces*, **5** 3370–3381 (2013)

10. Chhajed, S, Poxson, DJ, Yan, X, Cho, J, Schubert, EF, Welser, RE, Sood, AK, Kim, JK, "Nanostructured Multi-layer Tailored-Refractive-Index Antireflection Coating for Glass with Broadband and Omnidirectional Characteristics." *Appl. Phys. Exp.*, **4** 052503 (2011)

11. Wan, DH, Chen, HL, Tseng, TC, Fang, CY, Lai, YS, Yeh, FY, "Antireflective Nanoparticle Arrays Enhance the Efficiency of Silicon Solar Cells." *Adv. Funct. Mater*, **20** 3064–3075 (2010)

12. Olifierczuk, M, Zielinski, J, "Significance of Reflection Reduction in a TN Display for Colour Visualisation." *Opto Electron Rev.*, **10** 35–37 (2002)

13. Verma, L, Sakhuja, M, Son, J, Danner, A, Yang, H, Zeng, H, "Self-cleaning and Antireflective Packaging Glass for Solar Modules." *Renew. Energy*, **36** 2489–2493 (2011)

14. Kumar, PS, Sundaramurthy, J, Mangalaraj, D, Nataraj, D, Rajarathnam, D, Srinivasan, MP, "Enhanced Super-Hydrophobic and Switching Behavior of ZnO Nanostructured Surfaces Prepared by Simple Solution—Immersion Successive Ionic Layer Adsorption and Reaction Process." *J. Colloid Interface Sci.*, **363** 51–58 (2011)

15. Minemoto, T, Mizuta, T, Takakura, H, Hamakawa, Y, "Antireflective Coating Fabricated by Chemical Deposition of ZnO for Spherical Si Solar Cells." *Sol. Energy Mater. Sol. Cells*, **91** 191–194 (2007)

16. Swatowska, B, Stapinski, T, Drabczyk, K, Panek, P, "The Role of Antireflective Coatings in Silicon Solar Cells: The Influence on Their Electrical Parameters." *Opt. Appl.*, **41** 487–492 (2011)

17. Manca, M, Cannavale, A, DeMarco, L, Arico, AS, Cingolani, R, Gigli, G, "Durable Superhydrophobic and Antireflective Surfaces by Trimethylsilanized Silica Nanoparticles-Based Sol–Gel Processing." *Langmuir*, **25** 6357–6362 (2009)

18. Deng, X, Mammen, L, Zhao, Y, Lellig, P, Mullen, K, Li, C, "Transparent, Thermally Stable and Mechanically Robust Superhydrophobic Surfaces Made from Porous Silica Capsules." *Adv. Mater.*, **23** 2962–2965 (2011)

19. Bravo, J, Zhai, L, Wu, Z, Cohen, RE, Rubner, MF, "Transparent Superhydrophobic Films Based on Silica Nanoparticles." *Langmuir*, **23** 7293–7298 (2007)

20. Li, X, He, J, Liu, W, "Broadband Anti-reflective and Water-Repellent Coatings on Glass Substrates for Self-cleaning Photovoltaic Cells." *Mater. Res. Bull.*, **48** 2522–2528 (2013)

21. Chen, Y, Zhang, Y, Shi, L, Li, J, Xin, Y, Yang, T, "Transparent Superhydrophobic/Superhydrophilic Coatings for Self-cleaning and Anti-fogging." *Appl. Phys. Lett.*, **101** 033701 (2012)

22. Wang, G, Liang, W, Wang, B, Zhang, Y, Li, J, Shi, L, Guo, Z, "Conductive and Transparent Superhydrophobic Films on Various Substrates by In Situ Deposition." *Appl. Phys. Lett.*, **102** 203703 (2013)

23. Haque, SM, Rao, KD, Tripathi, S, De, R, Shinde, DD, Misal, JS, Prathap, C, Kumar, M, Som, T, Deshpande, U, Sahoo, NK, "Glancing Angle Deposition of SiO_2 Thin Films Using a Novel Collimated Magnetron Sputtering Technique." *Surf. Coat. Technol.*, **319** 61–69 (2017)

24. Mahadik, SA, Kavale, MS, Mukherjee, SK, Rao, AV, "Transparent Superhydrophobic Silica Coatings on Glass by Sol–Gel Method." *Appl. Surf. Sci.*, **257** 333–339 (2010)

25. Michels, AF, Soave, PA, Nardi, J, Jardim, PLG, Teixeira, SR, Weibel, DE, Horowitz, F, "Adjustable, (Super)hydrophobicity by E-beam Deposition of Nanostructured PTFE on Textured Silicon Surfaces." *J. Mater. Sci.*, **51** 1316–1323 (2016)

26. Singh, DP, Singh, JP, "Controlled Growth of Standing Ag Nanorod Arrays on Bare Si Substrate Using Glancing Angle Deposition for Self-cleaning Applications." *Appl. Phys. A Mater. Sci. Process.*, **104** 1189–1193 (2014)

27. Bruynooghe, S, Tonova, D, Sundermann, M, Koch, T, Schulz, U, "Antireflection Coatings Combining Interference Multilayers and a Nanoporous MgF$_2$ Top Layer Prepared by Glancing Angle Deposition." *Surf. Coat. Technol.*, **267** 40–44 (2015)

28. Lu, X, Kim, SM, Seo, SJ, "Fabrication of a Large-Area Superhydrophobic SiO$_2$ Nanorod Structured Surface Using Glancing Angle Deposition." *J. Nanomater.*, **2017** 8305439 (2017)

29. De, R, Misal, JS, Shinde, DD, Polaki, SR, Singh, R, Som, T, Sahoo, NK, Rao, KD, "A Fast and Facile Fabrication of PTFE Based Superhydrophobic and Ultra Wideband Angle Insensitive Anti-reflection Coatings." *Phys. Status Solidi RRL*, **12** 1800041 (2018)

30. De, R, Haque, SM, Misal, JS, Shinde, DD, Prathap, C, Polaki, SR, Som, T, Rao, KD, "Optical, Photocatalytic and Wetting Behavior of GLAD N$_2$-TiO$_2$ Films." *Phys. Status Solidi A*, **216** 1900021 (2019)

31. Fujiwara, H, *Spectroscopic Ellipsometry, Priciples and Applications*. Wiley, London (2007)

32. Kumar, V, Singh, N, Mehra, RM, Kapoor, A, Purohit, LP, Swart, HC, "Role of Film Thickness on the Properties of ZnO Thin Films Grown by Sol–Gel Method." *Thin Solid Films*, **539** 161–165 (2013)

33. Hawkeye, MM, Taschuk, MT, Brett, MJ, *Glancing Angle Deposition of Thin Films: Engineering the Nanoscale*, 1st ed. Wiley, London (2014)

34. Yan, X, Tong, X, Wang, J, Gong, C, Zhang, M, Liang, L, "Controllable Synthesis of Three-Dimensional Hierarchical Porous ZnO Film with Mesoporous Nanowalls." *Mater. Lett.*, **92** 165–168 (2013)

35. Bayer, IS, "On the Durability and Wear Resistance of Transparent Superhydrophobic Coatings." *Coatings*, **7** (1) 12 (2017)

36. Sutha, S, Suresh, S, Raj, B, Ravi, KR, "Transparent Alumina Based Superhydrophobic Self-cleaning Coatings for Solar Cell Cover Glass Applications." *Solar Energy Mater. Sol. Cells*, **165** 128–137 (2017)

37. Huang, JY, Li, SH, Ge, MZ, Wang, LN, Xing, TL, Chen, GQ, Liu, XF, Al-Deyab, SS, Zhang, KQ, Chen, T, Lai, YK, "Robust Superhydrophobic TiO$_2$@Fabrics for UV Shielding, Self-cleaning and Oil–Water Separation." *J. Mater. Chem. A*, **3** 2825–2832 (2015)

38. Wenzel, RN, "Surface Roughness and Contact Angle." *J. Phys. Chem.*, **53** 1466–1467 (1949)

39. Cassie, ABD, Baxter, S, "Wettability of Porous Surfaces." *Trans. Faraday Soc.*, **40** 546–551 (1944)

40. Horcas, I, Fernandez, R, Gomez-Rodriguez, JM, Colchero, J, Gomez-Herrero, J, Baro, AM, "WSXM: A Software for Scanning Probe Microscopy and a Tool for Nanotechnology." *Rev. Sci. Instrum.*, **78** 013705 (2007)